

WILEY-VCH



European Chemical  
Societies Publishing

# Take Advantage and Publish Open Access



By publishing your paper open access, you'll be making it immediately freely available to anyone everywhere in the world.

That's maximum access and visibility worldwide with the same rigor of peer review you would expect from any high-quality journal.

**Submit your paper today.**



[www.chemistry-europe.org](http://www.chemistry-europe.org)

# Base-free Oxidative Esterification of HMF over AuPd/nNiO-TiO<sub>2</sub>. When Alloying Effects and Metal-support Interactions Converge in Producing Effective and Stable Catalysts

Sebastiano Campisi,<sup>[a]</sup> Silvio Bellomi,<sup>[a]</sup> Lidia E. Chinchilla,<sup>[b]</sup> Laura Prati,<sup>[a]</sup> and Alberto Villa<sup>\*[a]</sup>

Furan-2,5-dimethylcarboxylate (FDMC), along with ethylene glycol (EG), is the key monomer to produce (poly-(ethylene-furanoate) (PEF). Noble metal-based catalysts can convert hydroxymethyl furfural (HMF) to FDMC in methanol through liquid phase catalytic oxidative esterification. In this work, the catalytic performance of Au, Pd and AuPd NPs supported on nanosized nickel oxide (nNiO) have been evaluated under base-free conditions at 90 °C and 3 bar O<sub>2</sub>. Synergistic effects

between Au and Pd imparted high activity and higher yield to FDMC compared to the monometallic counterparts. The role of support was also investigated by depositing AuPd NPs on TiO<sub>2</sub> and nNiO-TiO<sub>2</sub>. Remarkable yield to FDMC (85% after 8 h) and high stability were observed over AuPd/ nNiO-TiO<sub>2</sub> catalyst. This peculiar catalytic behavior could be imputed to the formation of trimetallic AuPdNi particles offering highly active interfacial sites.

## Introduction

The plastics industry is growing at a rapid pace. Plastic production reached nearly 370 million tons on a worldwide basis in 2019, according to a recent analysis.<sup>[1]</sup> The ever-more-widespread use in daily life, along with population growth and market expansion have contributed to the continuously rising demand for primary plastics. In addition, new specialty plastics are continually being developed to meet the need for emerging specific technical applications. Currently, petroleum-based polymers are still predominantly used in the plastics industry (low-density polyethylene LDPE, high-density polyethylene HDPE, polypropylene PP, polyvinylchloride PVC, polystyrene PS and polyethylene terephthalate PET).<sup>[2]</sup> From a sustainable and green perspective, these polymers have been criticized for their environmental issues and hazards related to present disposal methods, oil-dependency and difficult degradation. However, replacement of petroleum-based plastics is a challenging process. Under the green and circular economy stimuli, the plastic industry has been looking at using biomasses and their


derivatives as potential sources for monomers and polymers.<sup>[3,4]</sup> Poly(ethylene 2,5-furandicarboxylate) or polyethylene furanoate (PEF) represents a furan-based polyester that can be sourced from biomass and therefore it is a valid bio-based alternative to PET. The replacement of PET by PEF would lead to several advantages in terms of energy use, greenhouse gas (GHG) emissions, degradability (PEF films can undergo faster enzymatic hydrolysis compared to PET films). Furthermore, PEF possesses improved mechanical (e.g. tensile module) and thermal properties (high glass transition temperature), superior gas (O<sub>2</sub>, CO<sub>2</sub> and H<sub>2</sub>O) barrier properties than PET, and for this reason it is gaining growing attention for use in the food and beverage packaging industry.<sup>[3–5]</sup> PEF can be effectively obtained by condensation of ethylene glycol and 2,5-furandicarboxylic acid (FDCA) units. FDCA is a highly versatile and functional molecule that has been included among the twelve building blocks derived from biomass. Specifically, it can be easily synthesized through selective oxidation of hydroxymethyl furfural (HMF), a valuable platform chemical extracted from lignocellulosic biomass.<sup>[6]</sup>

Heterogeneously catalyzed oxidation of HMF with molecular oxygen (O<sub>2</sub>) or air is preferred over the use of stoichiometric oxidants or homogeneous catalysts (e.g. Co(OAc)<sub>2</sub> and Mn(OAc)<sub>2</sub> in AMOCO process<sup>[7]</sup>) for a more sustainable, energy saving and environmentally friendly process.<sup>[8,9]</sup> Almost quantitative yields to FDCA have been achieved over supported noble-metal (Au, Ru, Pd, Pt) nanoparticles as catalysts under relatively mild conditions in the presence of an alkaline medium.<sup>[10–14]</sup> Intensive research has been devoted to gain advanced insights on the reaction mechanism and to disclose the role of metal phase,<sup>[9,13,15–21]</sup> particle sizes,<sup>[22]</sup> support chemistry<sup>[19,23–29]</sup> and promoter addition<sup>[14,30,31]</sup> with the aim to optimize catalyst formulation and process conditions, with particular emphasis to the adoption of base-free conditions.<sup>[16,32–36]</sup> Nevertheless, the large scale production of FDCA under environmentally benign conditions and its use as

[a] Dr. S. Campisi, S. Bellomi, Prof. L. Prati, Prof. A. Villa  
Dipartimento di Chimica  
Università degli Studi di Milano  
Via Camillo Golgi, 19  
20133 Milano (Italy)  
E-mail: alberto.villa@unimi.it

[b] Dr. L. E. Chinchilla  
Departamento de Ciencia de los Materiales  
Ingeniería Metalúrgica y Química Inorgánica  
Facultad de Ciencias  
Universidad de Cádiz  
Campus Río San Pedro  
Puerto Real, E-11510 (Spain)

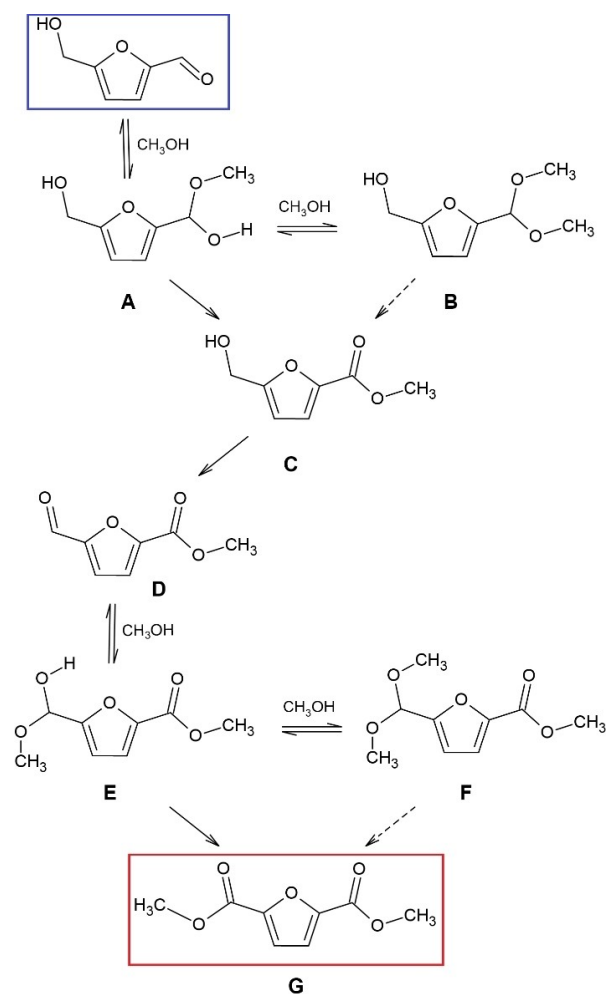
 Supporting information for this article is available on the WWW under <https://doi.org/10.1002/cctc.202200494>

 © 2022 The Authors. ChemCatChem published by Wiley-VCH GmbH. This is an open access article under the terms of the Creative Commons Attribution License, which permits use, distribution and reproduction in any medium, provided the original work is properly cited.

monomer for PEF synthesis is still hindered by some drawbacks associated with the large polarity, high boiling point, poor solubility of FDCA together with its tendency to undergo decomposition during the polymerization procedure, which results in a PEF product with undesirable color. An optimal solution could involve the replacement of FDCA by its corresponding dimethyl ester, i.e. furan-2,5-dimethylcarboxylate (FDMC), which can be directly employed in the fabrication of PEF by transesterification reaction with benefits in terms of cost-efficiency and technological solution. Indeed, FDMC can be synthesized by oxidative esterification of HMF in methanol, a solvent with higher volatility than water and then more easily separable in the course of polycondensation process. In addition, FDMC is characterized by good solubility in a large variety of solvents, relatively low boiling point and improved stability under polycondensation conditions, leading to a colorless PEF product. For all these reasons, the oxidative esterification to FDMC has recently moved into the limelight of research on chemo-catalytic processes for HMF upgrading to value-added chemicals. Although non-precious metal based catalysts, in particular Co-based and Mn-based systems, have been successfully proposed in the literature,<sup>[15,18,37–44]</sup> noble-metal based catalysts, specifically supported Au NPs, still remain the most studied catalysts for the oxidative esterification of HMF to FDMC.<sup>[10,26,45–55]</sup>

According to the literature, the reaction would proceed through an acetalization-oxidation-esterification mechanism (Scheme 1), although an alternative pathway involving alcohol oxidation to 2,5-diformylfuran (DFF) has been rarely reported.<sup>[18,37]</sup> The acetalization-oxidation-esterification mechanism implies the initial formation of a hemiacetal intermediate (A), which is unstable and cannot be detected by a gas chromatographic analysis. The hemiacetal can rapidly react following two different routes. In the former the hemiacetal is directly oxidized into the monoester alcohol (C), whereas the latter route entails the hemiacetal transformation into the acetal alcohol (2-furaldehyde-dimethyl-acetal, B), which may be then converted to the monoester alcohol (C). The alcohol function of C is then oxidized to form the monoester aldehyde (D), a highly unstable intermediate that rapidly undergo acetalization to form the hemiacetal ester (E), that, similarly to the hemiacetal A, can be directly converted to diester (FDMC, G) or undergo acetalization to acetal ester (F).

As in the case of the catalytic HMF oxidation to FDCA, the optimization of product distribution in the oxidative esterification requires a fine tuning and combination of several factors, including catalyst properties (catalyst support, particle size and shape, the active sites exposure) as well as process conditions (oxidant pressure, pH and HMF concentration). Unprecedented yield to FDMC can be achieved in alkaline media, as revealed by Christensen et al.,<sup>[10]</sup> who first proposed the use of Au/TiO<sub>2</sub> as catalysts for HMF oxidative esterification attaining 99% yield to FDMC. However, high yields to FDMC have been observed also under base-free conditions, as demonstrated by Corma et al. using Au/nCeO<sub>2</sub> catalyst.<sup>[49]</sup> In this case the combination of Au catalytic oxidative function and Lewis acid sites of ceria support promoted the reaction, which demonstrated to occur according



Scheme 1. Reaction pathways for HMF oxidative esterification.

to the pathway depicted in Scheme 1, where the oxidation of alcohol function was identified as the rate-determining step. Few years later, Manzoli et al.<sup>[50]</sup> performed tailored FT-IR measurements on Au/ZrO<sub>2</sub> which confirmed the hypotheses by Corma. According to Manzoli et al., the oxidative esterification over Au-based catalysts involved an oxygen sensitive and cooperative mechanism: the support promoted acetalization reaction while negatively charged Au clusters chemisorbed oxygen forming basic oxygen atoms which activated HMF and methanol molecules, by extracting H to originate alcoholate species. Furthermore, the same authors proved that functionalities and structure of the support also influence the shape of Au NPs with significant implications in the selectivity of the studied reaction.<sup>[51]</sup> More recently, Yuan et al.<sup>[52]</sup> reported remarkable yield to FDMC over optimized bimetallic AuCu/γ-Al<sub>2</sub>O<sub>3</sub> catalyst and ascribed such results to the presence of strongly interacting Au–CuO<sub>x</sub> interfacial sites which might act as the active sites. Synergistic effects were observed also in bimetallic AuPd NPs supported on Fe<sub>3</sub>O<sub>4</sub>, which demonstrated to be active and selective catalysts under alkaline conditions.<sup>[53]</sup>

Hence, based on previous evidences on the outstanding performances of Au, Pd and AuPd NPs supported on nanosized

nickel oxide (nNiO) in the base-free oxidation of HMF to FDCA,<sup>[36]</sup> this work investigates the catalytic performance of Au, Pd and AuPd NPs on nNiO, TiO<sub>2</sub> and mixed nNiO-TiO<sub>2</sub> supports in the base-free oxidative esterification of HMF, with the aim to unveil the synergistic effects deriving from the Au-Pd alloy formation and from metal-support interactions.

## Results and Discussion

Monometallic (Au and Pd) and bimetallic (AuPd, with optimized internal Au:Pd molar ratio of 6:4) nanoparticles were deposited on nNiO, TiO<sub>2</sub> and nNiO-TiO<sub>2</sub> supports by sol-immobilization procedure. X-ray photoelectron spectroscopy (XPS) data were collected to understand the surface chemistry and oxidation states of the catalyst species.

Evaluation of Au 4f data in Au and AuPd samples revealed the presence of one specie with binding energy (BE) 83.2–83.9 eV, which can be attributed to the presence of metallic Au (Table 1).<sup>[56]</sup> Evaluation of the Pd 3d for Pd and AuPd samples data showed the presence of two Pd 3d<sub>5/2</sub> species with binding energies of 335.1–335.7 and 336.9–337.4 eV attributed to Pd<sup>0</sup> and to oxidized Pd<sup>δ+</sup> respectively (Table 1). In all samples Pd is mainly present in the metallic form (76–88%) with a minority of oxidized Pd (12–24%) probably due to surface oxidation from the reaction with atmospheric O<sub>2</sub>.<sup>[57]</sup> After the addition of gold a slight negative shift in Au<sup>0</sup> binding energy from gold foil (84.0) is likely due to the interaction of Au-Pd due to the formation and presence of AuPd alloy nanoparticles with respect to the monometallic Au sample.<sup>[58,59]</sup> On the contrary, after the addition of gold no modifications in the Pd 3d<sub>3/2</sub> BE were detected, except when NiO-TiO<sub>2</sub> was used as the support. In this case also a shift of ~0.5 eV in Pd BE was envisaged. Moreover, in this sample, a higher content of Pd<sup>0</sup> in AuPd/nNiO-TiO<sub>2</sub> (88% and 12% for Pd<sup>0</sup> and Pd<sup>δ+</sup>, respectively Table 1) compared to the other Au-Pd catalysts (77–78% and 22–23% for Pd<sup>0</sup> and Pd<sup>δ+</sup>, respectively Table 1)

The Ni2p XPS data collected for the nNiO based catalysts reveals the presence of three Ni species (Table 1, Figure S1). The low energy Ni species (~854.5) can be attributed to the Ni-O bonds of nNiO. The peak centered at ~856 eV is due to the formation of Ni-OH, whereas the peak centered around 857.5 eV can be due to the formation of NiOOH. nNiO based catalysts showed similar Ni features, with the main presence of nNiO and NiOH, species. On the contrary, when nNiO was deposited on TiO<sub>2</sub> a higher contribution of Ni<sup>3+</sup> in the form of NiOOH was observed (27%).

The morphology of the prepared catalysts was analyzed by transmission electron microscopy (TEM). The detailed analysis of Au/nNiO, Pd/nNiO, AuPd/nNiO and AuPd/TiO<sub>2</sub> is reported in previous works.<sup>[36,60]</sup> nNiO nanoparticles were present in the form of 3–5 nm, with the presence of large, ordered agglomerates with a fraction of needle-like particles.<sup>[61]</sup> Au, Pd and AuPd are present as well dispersed nanoparticles in most cases, with a comparable particle size in the range of 3–5 nm (Table 1). Au/nNiO showed mean particle diameter of 4.5 nm (Table 1, Figure S.2) whereas smaller nanoparticles with a mean diameter of 3.6 nm were obtained for Pd/nNiO (Table 1, Figure S.3).<sup>[36]</sup> TEM analysis of AuPd/nNiO sample showed the presence of nanoparticles with a mean diameter of 3.3 nm (Table 1, Figure S.4). The EELS map confirms the presence of bimetallic nanoparticles with an enrichment of Pd around Au-Pd core particle. (S)TEM-EDS analysis confirms that all metal nanoparticles analyzed are alloy structures.<sup>[36]</sup> Alloyed Pd-Au particles with a mean size of 3.5 nm was also observed in the case of AuPd/TiO<sub>2</sub>.<sup>[62]</sup> When nNiO was deposited on TiO<sub>2</sub>, nNiO forms as nano crystalline thin sheets (the curled/folded edges of the sheets appear as dark needles in the TEM image) whereas the TiO<sub>2</sub> is primarily single crystal B20 nm cuboidal particles of both anatase and rutile crystallite.<sup>[63]</sup> EELS analysis showed the high density of Nickel particles distributed over the Titanium-rich crystal (Figure 1). Interestingly, the majority of the AuPd nanoparticles (average particle size of 3.2 nm) seems to be preferentially associated with the nNiO (Figure 1). EELS has been used to study the composition and nanostructure of bimetallic catalysts. The corresponding elemental map of Pd and Au reveals clearly the presence of both elements within the particle. Small amounts of Ni were found in the same region, probably partially covering the surface of the particle as can be seen in the elemental map (Figure 2). EELS line profiles of Pd-M5,4 Au-M4,5 and Ni-L3,2 taken across the nanoparticle are shown above. It can be noted the presence of two pronounced Ni signals at the center of the Np, whereas Au and Pd signals appears continuously across the entire particle, suggesting an alloy structure. The formation of a AuPdNi trimetallic system can be responsible of an electron transfer from Ni to AuPd and the shift in Pd BE.

In a previous work, some of the authors have demonstrated that supporting Au, Pd and AuPd NPs on nNiO resulted in effective catalysts for the base free oxidation of HMF under relatively low temperature (90 °C). In particular, AuPd/nNiO emerged for the remarkable yield to FDCA (70%) and the significant stability. These encouraging results suggested ex-

**Table 1.** XPS analyses and metal particle size measured by TEM.

Catalyst	XPS	Ni2p			Pd3d		Au4f	TEM Particle size [nm]
		BE [eV]	BE [eV]	BE [eV]	BE [eV]	BE [eV]	BE [eV]	
Au/nNiO	BE [eV]	854.3	856.0	857.3	–	–	83.9	4.5 ± 2.2 <sup>[a]</sup>
	[%]	50	42	8			100	
Pd/nNiO	BE [eV]	854.2	856.0	857.1	335.7	337.5	–	3.6 ± 0.8 <sup>[a]</sup>
	[%]	47	46	7	76	24	–	
AuPd/nNiO	BE [eV]	854.3	856.2	857.4	335.6	337.3	83.6	3.3 ± 1.1 <sup>[a]</sup>
	[%]	58	34	8	78	22	100	
AuPd/TiO <sub>2</sub>	BE [eV]	–	–	–	335.7	337.5	83.5	3.5 ± 1.2
	[%]	–	–	–	77	23	100	
AuPd/nNiO-TiO <sub>2</sub>	BE [eV]	854.5	856.1	857.5	335.1	336.9	83.2	3.2 ± 0.9
	[%]	35	38	27	88	12	100	

[a] Data from Ref. [36].



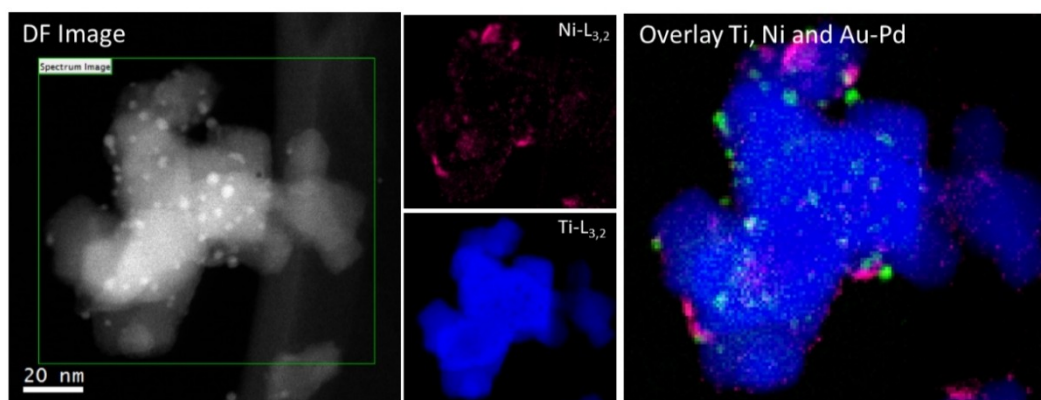


Figure 1. Representative micrograph of nNiO-TiO<sub>2</sub>, and EELS analysis showing the high density of Nickel particles distributed over the Titanium -rich crystal.

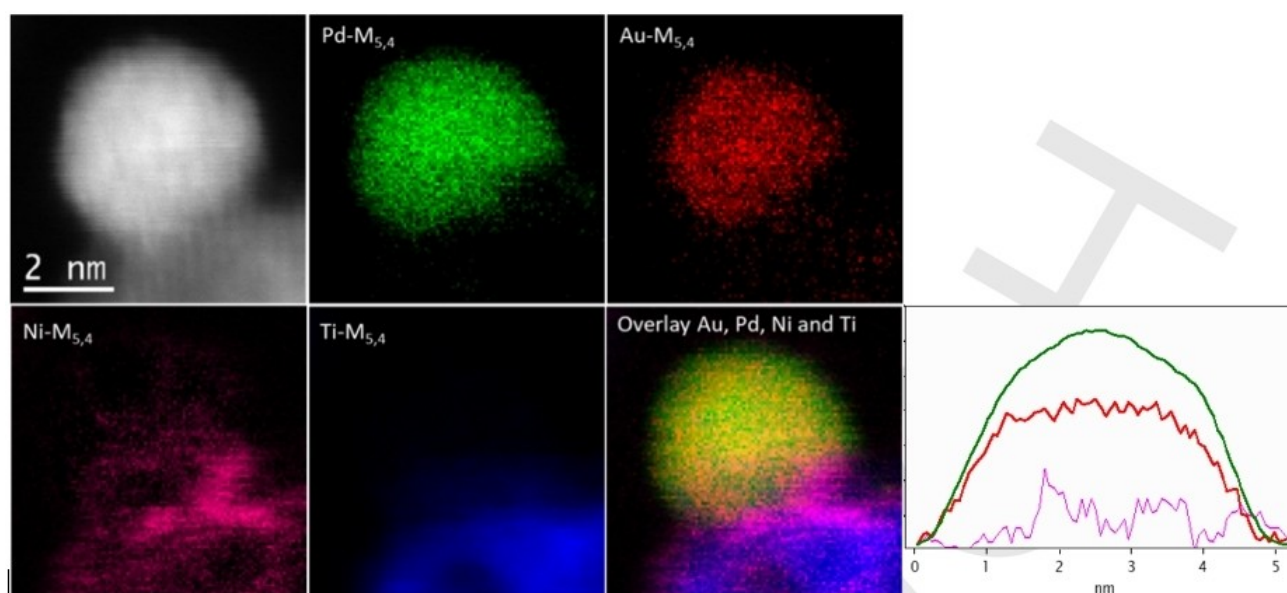


Figure 2. Elemental mapping of AuPd/nNiO-TiO<sub>2</sub> using electron energy loss spectroscopy (EELS)

ploring the potential of these catalysts also in the base-free oxidative esterification of HMF.

The catalytic performance in the oxidative esterification process was evaluated at 90 °C and under 3 bar oxygen pressure. The main results in terms of activity and selectivity are summarized in Table 2.

Focusing on the metal catalysts supported on nNiO, it is worth noting that all catalysts were active under the adopted experimental conditions, despite the absence of an alkaline environment. This evidence proves that nNiO enhances the catalytic properties of noble metal nanoparticles conferring activity even in base-free conditions, in a similar way to nanosized-CeO<sub>2</sub><sup>[49]</sup> and ZrO<sub>2</sub>.<sup>[50]</sup> The initial catalytic activity, defined as the HMF conversion rate per total moles of metal and calculated after 15 minutes of reaction, decreased in the order AuPd/nNiO (336 h<sup>-1</sup>) > Pd/nNiO (280 h<sup>-1</sup>) > Au/nNiO (168 h<sup>-1</sup>). The same trend was observed in the final conversion

**Table 2.** Catalytic testing results for the base-free oxidative esterification of hydroxymethyl furfural at 90 °C (A=hemiacetal intermediate, B=2-furaldehyde-dimethyl-acetal, C=monoester alcohol, D=monoester aldehyde E=hemiacetal ester, F=acetal ester, G=diester FDMC).

Catalyst <sup>[a]</sup>	Initial activity <sup>[b]</sup> [h <sup>-1</sup> ]	Con- version <sup>[c]</sup> [%]	Selectivity <sup>[d]</sup> [%]						
			A	B	C	D	E	F	G
Au/nNiO	168	81	–	20.8	10.0	–	–	26.7	38.5
Pd/nNiO	280	90	–	16.2	64.5	–	–	3.0	13.2
AuPd/ nNiO	336	95 <sup>[d]</sup>	–	1.8	0.3	–	–	41.9	53.8
AuPd/ TiO <sub>2</sub>	72	74	–	3.4	18.7	–	–	40.3	32.4
AuPd/ nNiO-TiO <sub>2</sub>	144	92	–	0.2	–	–	–	6.1	92.3

[a] Reaction conditions: HMF 0.3 M, metal/HMF 1/200, 90 °C, base-free, 3 bar O<sub>2</sub>; [b] Calculated as moles of converted HMF divided by reaction time (0.25 h) and total moles of metal, [c] After 8 h reaction time; [d] After 3 h reaction time.

after 8 h, specifically only 80% conversion was attained on Au/nNiO, while both AuPd/nNiO and Pd/nNiO were able to almost completely convert HMF, although over AuPd/nNiO HMF is quantitatively consumed after only 3 h, as shown in Figure 3a.

Looking at the selectivity after 8 h, as expected in all cases highly reactive hemiacetal products (A and E) were not detected, however important differences emerged in product distribution among Au, Pd and AuPd catalysts. In the case of Au/nNiO the diester (FDMC, G in Scheme 1) was the main product with a selectivity of 38.5%, which corresponds to a yield of 30.8%. This value is comparable to those obtained in the literature over Au/ZrO<sub>2</sub> and Au/sulf-ZrO<sub>2</sub> at 130 °C (Table S.1). Together with FDMC, no negligible amount of acetal alcohol (B, 21%) and acetal ester (F, 27%) were observed, while only 10% of monoester (C) was present. Conversely, the monoester C was the main final product (65%) when Pd/nNiO was used as catalyst. In this case the acetal alcohol (B) and the diester (G) were the main co-products with a selectivity of 16 and 13% respectively. A deeper insight on the selectivity and mechanism over Pd/nNiO may be gained by analyzing the evolution of product distribution as a function of the reaction time (Figure 3c). Actually, a close inspection of selectivity

profiles revealed that the diester (G) and the acetal ester (F) were the main products with selectivity values around 30–40%, within the first of reaction, when 60% of HMF is converted according to data in Figure 3a. After the first hour, HMF is still converted (albeit at lower conversion rate, as suggested by the decreased slope of the red curve in Figure 3a), but selectivity to diester and acetal ester declines, whereas the selectivity to monoester (C) increases. Such a behavior could be ascribed to a partial deactivation of Pd sites during the reaction. Indeed, it is known that the metal sites are responsible for oxidative steps, while the support promotes the acetalization reaction. Thus, it could be proposed that in the course of reaction, Pd active sites undergo deactivation and are no longer able to activate the alcohol function of the monoester C, which consequently cannot be further transformed to aldehyde ester (D), hemiacetal ester (E), acetal ester (F) and diester (G) and then accumulate, becoming the main detected product. The deactivation of Pd sites could be caused by metal leaching and overoxidation, as already reported in the literature for analogous Pd-based systems.<sup>[13,64]</sup>

Interestingly, in the presence of AuPd/nNiO the sum of diester, FDMC (G), and acetal ester (F) constituted more than

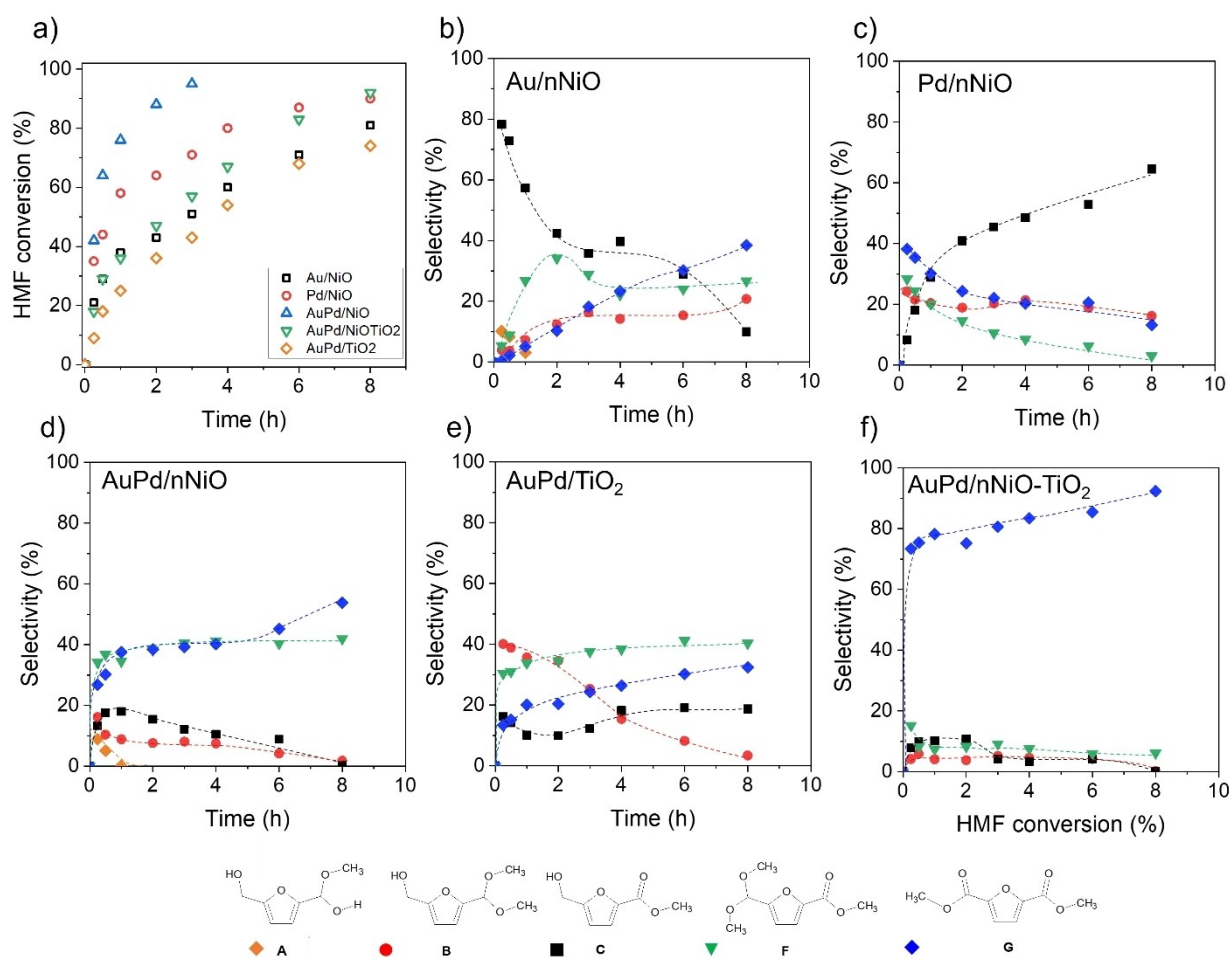


**Figure 3.** Effect of reaction time on (a) HMF conversion and on the selectivity of (b) Au/nNiO, (c) Pd/nNiO, (d) AuPd/nNiO, (e) AuPd/TiO<sub>2</sub> and (f) AuPd/nNiO-TiO<sub>2</sub>

95% of the detected products with selectivity of 54% and 42%, respectively. The good selectivity to FDMC and the high activity of AuPd/nNiO highlighted the beneficial impact of the alloy effects. Actually, the addition of Au to Pd imparted good activity and high resistance to deactivation. Such a synergistic effect has been already observed in the literature and has been tentatively ascribed to both geometric (e.g. site isolation) and electronic effects.<sup>[65]</sup> Regarding the formation of acetals (B and F), it should be emphasized that the origin and the role of acetals in the mechanism of oxidative esterification is still debated in the literature. Indeed, although most of literature studies agree in ruling out the involvement of acetals as intermediates for the formation of mono- and diester, some recent reports<sup>[47]</sup> hypothesized that also acetals could undergo transformation to esters. However, product distribution profiles of Au/nNiO and AuPd/nNiO in Figure 3, b and d, showed that on these catalysts the selectivity to acetals remained stable over the time, while selectivity to diester increased, thus suggesting that acetals are stable byproducts. In any case, the formation of stable acetals over AuPd/nNiO affected in some extent the yield to diester and for this reason their origin under reaction conditions deserved to be further investigated with the aim to minimize their formation. Several factors have been reported to contribute to acetal formation, such as particle size (acetal is formed on Au with size  $d > 4$  nm),<sup>[66]</sup> basic site depletion<sup>[45]</sup> and presence of strong Lewis acid sites.<sup>[50]</sup> Considering that metal nanoparticle size in the studied catalysts in  $< 4$  nm, this factor can be excluded. The formation of acetal could be then associated with peculiar acid/base surface properties of nNiO. Indeed, according to previous reports, nNiO has a pronounced basic character with basic site density of  $0.21 \text{ mmol g}^{-1}$ , as determined by liquid phase titration.<sup>[61]</sup> To unravel the role of the support in promoting acetal formation, AuPd NPs were supported onto TiO<sub>2</sub> and nNiO-TiO<sub>2</sub> (10:90 wt/wt ratio) supports and the resulting catalysts were tested in the base-free oxidative esterification of HMF. Initial activity data in Table 2 provided important information on role of support. On one side, AuPd/TiO<sub>2</sub> exhibited initial activity value ( $72 \text{ h}^{-1}$ ) five times lower than AuPd/nNiO ( $336 \text{ h}^{-1}$ ). On the other side a modest percentage of nNiO (10 wt.%) is sufficient to lead the activity to be twice as high ( $144 \text{ h}^{-1}$ ), thus confirming the peculiar catalytic behavior of nNiO. Interestingly, despite its lower initial activity compared to AuPd/nNiO, AuPd/nNiO-TiO<sub>2</sub> assured almost complete HMF conversion after 8 h (92%). However, the most striking fact is the unique selectivity to FDMC (92%) on AuPd/nNiO-TiO<sub>2</sub>. Actually, the yield to FDMC was significantly higher over AuPd/nNiO-TiO<sub>2</sub> (85%) than over the other bimetallic catalysts (Figure 4a).

Although higher values of yield to FDMC have been reported in the literature over Au-based catalysts (Table S.1), the result here obtained on AuPd/nNiO-TiO<sub>2</sub> is of great importance, since it has been obtained under mild conditions (absence of base,  $90^\circ\text{C}$ , 3 bar O<sub>2</sub>). Moreover, recycling tests proved that AuPd/nNiO-TiO<sub>2</sub> is also highly stable and maintains initial activity, conversion and selectivity over six runs (Figure 3b). The good stability of AuPd/nNiO-TiO<sub>2</sub> was confirmed by additional TEM and XPS characterization on the catalyst after

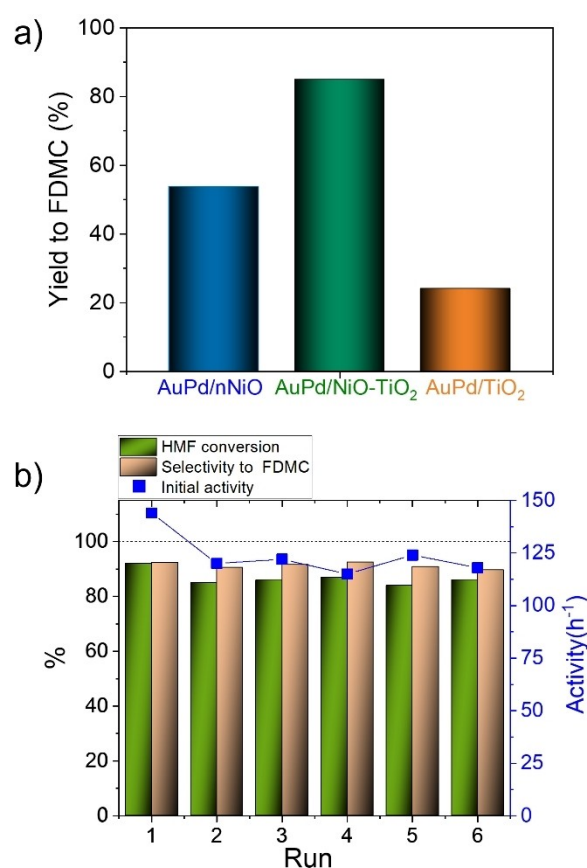


**Figure 4.** a) Yield to FDMC over bimetallic AuPd catalysts ( $90^\circ\text{C}$ , base-free, 3 bar O<sub>2</sub>, 8 h); b) stability tests results on AuPd/nNiO-TiO<sub>2</sub> Reaction conditions: HMF 0.3 M, metal/HMF 1/200,  $90^\circ\text{C}$ , base-free, 3 bar O<sub>2</sub>, 8 h.

use. The analyses (Table S.2) demonstrated that the metal phase was not modified after testing, since original particle size and oxidation states were maintained. Slight difference was observed in the electronic state of Ni: fitting of the Ni2p<sub>3/2</sub> XP spectrum showed a decrease in the fraction of low energy Ni species at 854.5 eV (from 35% to 26%) and simultaneous increase (from 27 to 41%) of the component at 857.5 eV associated with Ni<sup>3+</sup>-(O)OH species. The oxidation of Ni<sup>3+</sup> can be ascribed to O atoms origination from O<sub>2</sub> dissociation, as already reported in previous works.<sup>[61]</sup>

The unique catalytic performance of AuPd/nNiO-TiO<sub>2</sub> could be rationalized by considering the information from XPS and TEM-EELS characterization. In particular, EELS analyses evidenced the formation of Ni-decorated AuPd nanoparticles AuPd/nNiO-TiO<sub>2</sub>. The presence of dispersed Ni-phase in intimate contact with AuPd surface might result in a greater number of interface sites, which are known to be active sites in the Au-catalyzed oxidative esterification. In addition, the nickel phase migrated at the surface of AuPd NPs could be associated with NiOOH species, which are predominant in AuPd/nNiO-TiO<sub>2</sub> according to XPS characterization. Such NiOOH species have been demonstrated to be highly active in the electrocatalytic production of oxygen from water<sup>[67,68]</sup> and have been also predicted to promote the oxidative dehydrogenation of



alkane.<sup>[69]</sup> Additionally, the presence of NiOOH has been associated with high yield to methyl lactate in the fructose esterification reaction over nNiO catalysts.<sup>[70]</sup> Based on these considerations, the high activity and selectivity to FDMC of AuPd/nNiO-TiO<sub>2</sub> can be ascribed to the interfacial sites where the complete oxidative esterification of HMF is promoted by the co-presence of NiOOH sites facilitating the acetalization reaction and metal sites responsible for hemiacetal oxidation (Scheme 2).

## Conclusion

Monometallic (Au, Pd) and bimetallic (AuPd) were successfully deposited onto nNiO through the sol immobilization procedure. The catalytic oxidative esterification of HMF with methanol was performed in base-free conditions at 90 °C with 3 bar O<sub>2</sub>. The synergistic effect between Au and Pd substantially enhanced the initial activity (336 h<sup>-1</sup>), improved the resistance to deactivation and influenced the product distribution.

Bimetallic AuPd NPs were also supported onto TiO<sub>2</sub> and nNiO-TiO<sub>2</sub> to study the effect of support.

Catalytic tests revealed that the support markedly influenced the catalytic performance. In particular, best results (85% yield to FDMC after 8 h, stability over 6 runs) were attained over AuPd/nNiO-TiO<sub>2</sub> catalyst. XPS and TEM-EELS characterization allowed to explore the structure–activity relationships. Results suggested that the presence of highly dispersed Ni-phase (likely in the form of NiOOH clusters) over AuPd NPs might generate active interfacial sites, responsible for the unique catalytic performance of AuPd/nNiO-TiO<sub>2</sub> catalyst. Although further investigation by *in situ* characterization and theoretical simulations are still needed for a full understanding of the mechanistic aspects and of the structure of catalytically active sites, the present study on bimetallic AuPd catalysts for the oxidative esterification of HMF may provide some guidance for

the preparation of active, selective and stable catalysts for biomass upgrading.

## Experimental Section

### Support preparation

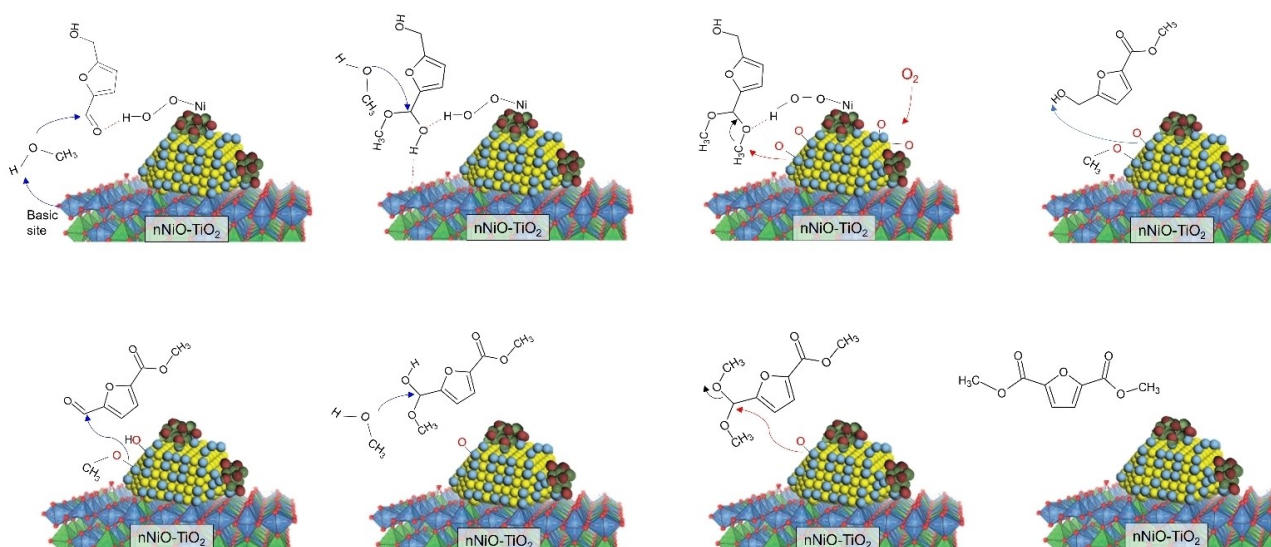
**nNiO:** nNiO was prepared according to the procedure described elsewhere. Ni(NO<sub>3</sub>)<sub>2</sub>·6H<sub>2</sub>O (5 × 10<sup>-4</sup> M) (Sigma-Aldrich, purity > 99.9%) and urea (Sigma-Aldrich, purity > 99.5%) (Ni/urea molar ratio 1:10 mol/mol) were mixed into 0.2 L of MilliQ water under magnetic stirring. The solution was maintained under stirring for 6 h at 80 °C. The precipitated Ni(OH)<sub>2</sub> was separated from the solution by filtration and washed several times. The powder was dried at 60 °C for 12 h and then calcined at 300 °C for 3 h in static air.

**nNiO/TiO<sub>2</sub>:** The nNiO/TiO<sub>2</sub> support was prepared by depositing a proper amount of nanometric NiO (10 wt%) on TiO<sub>2</sub> (90 wt%, Degussa P25) by adding the above 5 × 10<sup>-4</sup> M Ni(NO<sub>3</sub>)<sub>2</sub>·6H<sub>2</sub>O acting as a NiO precursor to a suspension of TiO<sub>2</sub>. To confirm the nominal ratio, the elemental composition of NiO<sub>10</sub>-TiO<sub>2</sub><sub>90</sub> was measured by X-ray fluorescence.

### Monometallic catalyst preparation

**Au-nNiO:** Solid NaAuCl<sub>4</sub>·2H<sub>2</sub>O (51 μmol) and polyvinyl alcohol (PVA, 1 wt%) solution (Au:PVA mass ratio of 2:1 wt/wt) were introduced in 0.1 L of MilliQ water. After 5 min, a fresh solution of NaBH<sub>4</sub> (0.1 M) (Au:NaBH<sub>4</sub> 1:4 mol/mol) was added to the solution under stirring, resulting in the rapid formation of Au(0) sol. Within a few minutes of sol generation, colloidal nanoparticles were immobilized by adding the support under vigorous stirring. The amount of support was calculated to achieve a total final nominal metal loading of 1 wt%, as verified by ICP analysis. After 2 h the slurry was filtered, and the catalyst was washed thoroughly with distilled water and dried at 80 °C for 4 h.

**Pd-nNiO:** Solid Na<sub>2</sub>PdCl<sub>4</sub>·2H<sub>2</sub>O (51 μmol) and PVA (1 wt%) solution (Pd:PVA mass ratio of 2:1 wt/wt) were added to 0.1 L of MilliQ water. After 5 min, a fresh solution of NaBH<sub>4</sub> (0.1 M) (Pd:NaBH<sub>4</sub>



**Scheme 2.** Possible reaction mechanism for HMF oxidative esterification over AuPd/nNiO-TiO<sub>2</sub>.



1:8 mol/mol) was added to the solution under stirring and a Pd(O) sol was generated. Within a few minutes of sol formation, the colloid was immobilized by adding the support under vigorous stirring. The amount of support was calculated to attain a total final nominal metal loading of 1 wt%, as verified by ICP analysis. After 2 h the slurry was filtered, and the catalyst was washed thoroughly with distilled water and dried at 80 °C for 4 h.

### Bimetallic catalyst preparation

**AuPd-nNiO, AuPd/TiO<sub>2</sub> and AuPd/NiO-TiO<sub>2</sub>.** Solid NaAuCl<sub>4</sub>·2H<sub>2</sub>O (31 μmol) and Na<sub>2</sub>PdCl<sub>4</sub>·2H<sub>2</sub>O (20 μmol) (Au:Pd molar ratio of 6:4 mol/mol) and 1 wt% PVA solution (Pd:PVA mass ratio of 2:1 wt/wt) were added to 0.1 L of MilliQ water. After 5 min, a fresh solution of NaBH<sub>4</sub> (0.1 M) (Pd:NaBH<sub>4</sub> molar ratio of 1:8 mol/mol) was added to the solution under stirring. Within a few minutes of sol generation, the colloid was immobilized by adding the support under vigorous stirring. The amount of support was calculated as having a total final nominal metal loading of 1 wt%, as verified by ICP analysis. After 2 h the solid was recovered from the slurry by filtration, washed thoroughly with distilled water and dried at 80 °C for 4 h. After washing, the intensity of C 1s signal significantly decreased (Figure S5), confirming the almost complete removal of the protecting agent.

### Catalyst characterization

**TEM:** Samples for transmission electron microscopy (TEM) studies were prepared by depositing small amounts of dry catalyst powder onto holey carbon copper grids. Micrographs combined with analytical studies by energy-dispersive X-ray (XEDS) and electron energy loss spectroscopy were performed in High Annular Dark Field mode using a FEI Titan3 80–300 microscope operated at 80 kV. Digital Micrograph, TIA, and INCA software's were used for the analysis of the TEM micrographs and XEDS spectra. The PSD, Gaussian fit, average particle diameter, and metal dispersion were calculated assuming a truncated cubooctahedron particle shape using Gauss software. EELS data including drift correction base on the zero-loss peak, background subtraction, and principal component analysis (PCA), were processed using Gatan's Digital Micrograph and Hyperspy software's.

**XPS:** X-ray photoelectron spectroscopy (XPS) data were collected using a PHI 3056 XPS with an Al anode source operated at 15 kV and an applied power of 350 W. The energy scale calibration of the instrument is checked using a sputter cleaned piece of Ag. The lowest C1s BE species were shifted about 0.1 eV to 284.8 eV for comparison to literature values. Surface concentrations are calculated by integrating the peaks area and using standard atomic sensitivity factors supplied by the equipment manufacturer. The spectra were deconvoluted using Gaussian-Lorentzian functions and a Shirley-type background.

**Composition:** Atomic Absorption Spectroscopy (AAS). The metal content was checked by AAS analysis of the filtrate on a Perkin Elmer 3100 instrument. After the catalyst filtration, 10 ml sample of the filtered solution was collected and analyzed.

### Catalytic tests

The catalytic tests were performed in a lab scale autoclave reactor (100 mL capacity from Parr), equipped with a mechanical stirrer and sensors for measuring temperature and pressure. The solution of HMF (0.3 M, 25 mL in methanol) and catalyst (HMF/total metal molar ratio=200) were loaded in the reactor. HMF (purity > 99%)

was purchased from AVABiochem and used without any purification.

The autoclave reactor was purged 3 times with O<sub>2</sub> and then pressurized at 3 bar. The temperature was increased to the set point (90 °C) and the reaction mixture was stirred at 1200 rpm for the whole duration of the experiment. Initial time (time zero) for the reaction was considered when the set point temperature was reached (after 10 min). At the end of the reaction, the reactor was cooled down to room temperature and the solution was filtered. Samples were removed periodically (0.2 mL) and HP 7820 A gas chromatograph equipped with a capillary column HP-5 30 m × 0.32 mm, 0.25 μm Film, by Agilent Technologies. Authentic samples were analyzed to determine separation times. Quantitative analyses with external standard method (dodecanol) were used. Products were identified using gas chromatograph-mass spectroscopy (GC-MS). Aliquots of the reaction mixture were analyzed using a Thermo Scientific ISQ QD, equipped with an Agilent VF-5 ms column, 60 m × 0.32 mm × 1 μm (inner diameter thickness). Recycling tests have been performed by reusing the recovered catalyst without any further cleaning procedure.

### Acknowledgements

Open Access Funding provided by Universita degli Studi di Milano within the CRUI-CARE Agreement.

### Conflict of Interest

The authors declare no conflict of interest.

### Data Availability Statement

Research data are not shared.

**Keywords:** base-free · bioplastics · cooperative catalysis · synergistic effect · trimetallic particles

- [1] Plastic Europe - Association of Plastics Manufacturers, "Plastics – the Facts 2020," 2020.
- [2] S. Brockhaus, M. Petersen, W. Kersten, *J. Cleaner Prod.* **2016**, *127*, 84–95.
- [3] H. Nakajima, P. Dijkstra, K. Loos, *Polymers (Basel)*. **2017**, *9*, 1–26.
- [4] K. R. Hwang, W. Jeon, S. Y. Lee, M. S. Kim, Y. K. Park, *Chem. Eng. J.* **2020**, *390*, 124636.
- [5] L. Maini, M. Gigli, M. Gazzano, N. Lotti, D. N. Bikiaris, G. Z. Papageorgiou, *Polymers (Basel)*. **2018**, *10*, DOI 10.3390/polym10030296.
- [6] Y. Wan, J.-M. Lee, *ChemSusChem* **2021**, *n/a*, DOI 10.1002/cssc.202102041.
- [7] W. Partenheimer, V. V. Grushin, *Adv. Synth. Catal.* **2001**, *343*, 102–111.
- [8] M. Sajid, X. Zhao, D. Liu, *Green Chem.* **2018**, *20*, 5427–5453.
- [9] D. Zhao, T. Su, Y. Wang, R. S. Varma, C. Len, *J. Mol. Catal.* **2020**, *495*, 111133.
- [10] E. Taarning, I. S. Nielsen, K. Egeblad, R. Madsen, C. H. Christensen, *ChemSusChem* **2008**, *1*, 75–78.
- [11] O. Casanova, S. Iborra, A. Corma, *ChemSusChem* **2009**, *2*, 1138–1144.
- [12] S. E. Davis, L. R. Houk, E. C. Tamargo, A. K. Datye, R. J. Davis, *Catal. Today* **2011**, *160*, 55–60.
- [13] A. Villa, M. Schiavoni, S. Campisi, G. M. Veith, L. Prati, *ChemSusChem* **2013**, *6*, 609–612.
- [14] H. Ait Rass, N. Essayem, M. Besson, *ChemSusChem* **2015**, *8*, 1206–1217.

- [15] X. Tong, L. Yu, H. Chen, X. Zhuang, S. Liao, H. Cui, *Catal. Commun.* **2017**, *90*, 91–94.
- [16] H. Chen, J. Shen, K. Chen, Y. Qin, X. Lu, P. Ouyang, J. Fu, *Appl. Catal. A* **2018**, *555*, 98–107.
- [17] O. R. Schade, K. F. Kalz, D. Neukum, W. Kleist, J. D. Grunwaldt, *Green Chem.* **2018**, *20*, 3530–3541.
- [18] A. Salazar, P. Hünemörder, J. Rabeah, A. Quade, R. V. Jagadeesh, E. Mejia, *ACS Sustainable Chem. Eng.* **2019**, *7*, 12061–12068.
- [19] H. F. Pérez-Bustos, C. J. Lucio-Ortiz, J. R. de la Rosa, D. A. de Haro del Río, L. Sandoval-Rangel, D. X. Martínez-Vargas, C. S. Maldonado, V. Rodríguez-González, M. A. Garza-Navarro, F. J. Morales-Leal, *Fuel* **2019**, *239*, 191–201.
- [20] A. Tirsoaga, M. El Fergani, N. Nuns, P. Simon, P. Granger, V. I. Parvulescu, S. M. Coman, *Appl. Catal. B* **2020**, *278*, 119309.
- [21] T. W. Chamberlain, V. Degirmenci, R. I. Walton, *ChemCatChem* **2022**, *100*, DOI 10.1002/cctc.202200135.
- [22] C. Megías-Sayago, A. Lolli, D. Bonincontro, A. Penkova, S. Albonetti, F. Cavani, J. A. Odriozola, S. Ivanova, *ChemCatChem* **2020**, *12*, 1177–1183.
- [23] Y. Wei, Y. Zhang, Y. Chen, F. Wang, Y. Cao, W. Guan, X. Li, *ChemSusChem* **2021**, *14*, 1–12.
- [24] Q. Li, H. Wang, Z. Tian, Y. Weng, C. Wang, J. Ma, C. Zhu, W. Li, Q. Liu, L. Ma, *Catal. Sci. Technol.* **2019**, *9*, 1570–1580.
- [25] C. Megías-Sayago, A. Lolli, S. Ivanova, S. Albonetti, F. Cavani, J. A. Odriozola, *Catal. Today* **2019**, *333*, 169–175.
- [26] D. K. Mishra, J. K. Cho, Y. Yi, H. J. Lee, Y. J. Kim, *J. Ind. Eng. Chem.* **2019**, *70*, 338–345.
- [27] D. German, E. Pakrieva, E. Kolobova, S. A. C. Carabineiro, M. Stucchi, A. Villa, L. Prati, N. Bogdanchikova, V. Cortés Corberán, A. Pestryakov, *Catalysts* **2021**, *11*, 115.
- [28] R. Chen, J. Xin, D. Yan, H. Dong, X. Lu, S. Zhang, *ChemSusChem* **2019**, *12*, 2715–2724.
- [29] Z. Gui, W. Cao, S. Saravanamurugan, A. Riisager, L. Chen, Z. Qi, *ChemCatChem* **2016**, *8*, 3636–3643.
- [30] H. Ait Rass, N. Essayem, M. Besson, *Green Chem.* **2013**, *15*, 2240–2251.
- [31] X. Jia, J. Ma, M. Wang, Z. Du, F. Lu, F. Wang, J. Xu, *Appl. Catal. A* **2014**, *482*, 231–236.
- [32] L. Ardemani, G. Cibir, A. J. Dent, M. A. Isaacs, G. Kyriakou, A. F. Lee, C. M. A. Parlett, S. A. Parry, K. Wilson, *Chem. Sci.* **2015**, *6*, 4940–4945.
- [33] J. Artz, R. Palkovits, *ChemSusChem* **2015**, *8*, 3832–3838.
- [34] D. K. Mishra, H. J. Lee, J. Kim, H.-S. Lee, J. K. Cho, Y.-W. Suh, Y. Yi, Y. J. Kim, *Green Chem.* **2017**, *19*, 1619–1623.
- [35] S. Campisi, S. Capelli, D. Motta, F. Trujillo, T. Davies, L. Prati, N. Dimitratos, A. Villa, *C — Journal of Carbon Research* **2018**, *4*, 48.
- [36] D. Bonincontro, A. Lolli, A. Villa, L. Prati, N. Dimitratos, G. M. Veith, L. E. Chinchilla, G. A. Botton, F. Cavani, S. Albonetti, *Green Chem.* **2019**, *21*, 4090–4099.
- [37] J. Deng, H.-J. Song, M.-S. Cui, Y.-P. Du, Y. Fu, *ChemSusChem* **2014**, *7*, 3334–3340.
- [38] Y. Sun, H. Ma, X. Jia, J. Ma, Y. Luo, J. Gao, J. Xu, *ChemCatChem* **2016**, *8*, 2907–2911.
- [39] K. S. Kozlov, L. V. Romashov, V. P. Ananikov, *Green Chem.* **2019**, *21*, 3464–3468.
- [40] H. Zhou, S. Hong, H. Zhang, Y. Chen, H. Xu, X. Wang, Z. Jiang, S. Chen, Y. Liu, *Appl. Catal. B* **2019**, *256*, 117767.
- [41] K. K. Sun, S. J. Chen, Z. L. Li, G. P. Lu, C. Cai, *Green Chem.* **2019**, *21*, 1602–1608.
- [42] Y. Lin, G. P. Lu, X. Zhao, X. Cao, L. Yang, B. Zhou, Q. Zhong, Z. Chen, *J. Mol. Catal.* **2020**, *482*, 110695.
- [43] T. Rui, G. P. Lu, X. Zhao, X. Cao, Z. Chen, *Chin. Chem. Lett.* **2021**, *32*, 685–690.
- [44] Y. Feng, S. Long, G. Yan, W. Jia, Y. Sun, X. Tang, Z. Zhang, X. Zeng, L. Lin, *J. Catal.* **2021**, *397*, 148–155.
- [45] C. P. Ferraz, A. H. Braga, M. N. Ghazzal, M. Zieliński, M. Pietrowski, I. Itabaiana, F. Dumeignil, L. M. Rossi, R. Wojcieszak, *Catalysts* **2020**, *10*, 430.
- [46] H. Weerathunga, S. Sarina, H. Y. Zhu, E. R. Waclawik, *ACS Omega* **2021**, *6*, 4740–4748.
- [47] Z. Shahin, F. Rataboul, A. Demessence, *J. Mol. Catal.* **2021**, *499*, 111265.
- [48] M. Manzoli, F. Menegazzo, M. Signoretto, D. Marchese, *Catalysts* **2016**, *6*, DOI 10.3390/catal6070107.
- [49] O. Casanova, S. Iborra, A. Corma, *J. Catal.* **2009**, *265*, 109–116.
- [50] F. Menegazzo, T. Fantinel, M. Signoretto, F. Pinna, M. Manzoli, *J. Catal.* **2014**, *319*, 61–70.
- [51] F. Menegazzo, M. Signoretto, D. Marchese, F. Pinna, M. Manzoli, *J. Catal.* **2015**, *326*, 1–8.
- [52] J. Du, H. Fang, H. Qu, J. Zhang, X. Duan, Y. Yuan, *Appl. Catal. A* **2018**, *567*, 80–89.
- [53] M. Kim, Y. Su, A. Fukuoka, E. J. M. Hensen, K. Nakajima, *Angew. Chem. Int. Ed.* **2018**, *57*, 8235–8239; *Angew. Chem.* **2018**, *130*, 8367–8371.
- [54] A. Buonerba, S. Impemba, A. D. Litta, C. Capacchione, S. Milione, A. Grassi, *ChemSusChem* **2018**, *11*, 3139–3149.
- [55] A. Cho, S. Byun, J. H. Cho, B. M. Kim, *ChemSusChem* **2019**, *12*, 2310–2317.
- [56] G. M. Veith, A. R. Lupini, N. J. Dudney, *J. Phys. Chem. C* **2009**, *113*, 269–280.
- [57] E. H. Voogt, A. J. M. Mens, O. L. J. Gijzeman, J. W. Geus, *Surf. Sci.* **1997**, *373*, 210–220.
- [58] J. Radnik, C. Mohr, P. Claus, *Phys. Chem. Chem. Phys.* **2003**, *5*, 172–177.
- [59] M. P. Casaletto, A. Longo, A. Martorana, A. Prestianni, A. M. Venezia, *Surf. Interface Anal.* **2006**, *38*, 215–218.
- [60] A. Villa, D. Ferri, S. Campisi, C. E. Chan-Thaw, Y. Lu, O. Kröcher, L. Prati, *ChemCatChem* **2015**, *7*, 2534–2541.
- [61] A. Villa, C. E. Chan-Thaw, G. M. Veith, K. L. More, D. Ferri, L. Prati, *ChemCatChem* **2011**, *3*, 1612–1618.
- [62] C. E. Chan-Thaw, A. Villa, G. M. Veith, L. Prati, *ChemCatChem* **2015**, *7*, 1338–1346.
- [63] A. Villa, G. M. Veith, D. Ferri, A. Weidenkaff, K. A. Perry, S. Campisi, L. Prati, *Catal. Sci. Technol.* **2013**, *3*, 394–399.
- [64] S. Campisi, C. E. Chan-Thaw, L. E. Chinchilla, A. Chutia, G. A. Botton, K. M. H. Mohammed, N. Dimitratos, P. P. Wells, A. Villa, *ACS Catal.* **2020**, *10*, 5483–5492.
- [65] A. Villa, D. Wang, D. S. Su, L. Prati, *Catal. Sci. Technol.* **2015**, *5*, 55–68.
- [66] F. Pinna, A. Olivo, V. Trevisan, F. Menegazzo, M. Signoretto, M. Manzoli, F. Boccuzzi, *Catal. Today* **2013**, *203*, 196–201.
- [67] J. M. P. Martínez, E. A. Carter, *Chem. Mater.* **2018**, *30*, 5205–5219.
- [68] L. F. Li, Y. F. Li, Z. P. Liu, *ACS Catal.* **2020**, *10*, 2581–2590.
- [69] L. Li, H. Wang, J. Han, X. Zhu, Q. Ge, *Trans. Tianjin Univ.* **2020**, *26*, 341–351.
- [70] X. Lyu, L. Xu, J. Wang, X. Lu, *Catal. Commun.* **2019**, *119*, 46–50.

Manuscript received: April 11, 2022  
Accepted manuscript online: May 9, 2022  
Version of record online: June 7, 2022